Tuning the competing phases of bilayer ruthenate Ca_{3}Ru_{2}O_{7} via dilute Mn impurities and magnetic field

M. Zhu, J. Peng, W. Tian, T. Hong, Z. Q. Mao, and X. Ke

Phys. Rev. B **95**, 144426 — Published 21 April 2017

DOI: 10.1103/PhysRevB.95.144426

Tuning the competing phases of bilayer ruthenate $Ca_3Ru_2O_7$ via dilute Mn impurities and magnetic field

M. Zhu[1], J. Peng[2], W. Tian[3], T. Hong[3], Z. Q. Mao[4], and X. Ke[1*]

[1]*Department of Physics and Astronomy, Michigan State University, East Lansing, Michigan 48824, USA*

[2]*Collaborative Innovation Center of Advanced Microstructures, Lab of Solid State Microstructures, School of Physics, Nanjing University, Nanjing 210093, People's Republic of China*

[3]*Quantum Condensed Matter Division, Oak Ridge National Laboratory, Oak Ridge, Tennessee 37831, USA*

[4]*Department of Physics and Engineering Physics, Tulane University, New Orleans, Louisiana 70118, USA*

* Correspondence to: ke@pa.msu.edu

We have systematically investigated the evolution of the magnetic structure of the bilayer ruthenate $Ca_3(Ru_{1-x}Mn_x)_2O_7$ induced upon Mn doping. For $0 < x \leq 0.03$ the materials exhibit the same spin structure as that of the parent compound at low temperature, while an incommensurate cycloidal magnetic structure emerges at T slightly above the metal-insulator transition temperature (T_{MIT}). In contrast, for $x \geq 0.04$ the ground state becomes a G-type antiferromagnetic Mott insulator. Furthermore, we have observed magnetic-field-induced transitions in $Ca_3(Ru_{0.96}Mn_{0.04})_2O_7$ which is positioned at the phase boundary. Below T_{MIT}, the magnetic transition is accompanied by a structural transition, as well as a dramatic change in the electronic properties from a Mott insulator to a localized phase. On the contrary, an incommensurate-to-commensurate spin structure transition is observed for $T_{MIT} < T < T_{ICM}$. Our results suggest strong competing magnetic tendencies in this bilayer ruthenate system that are very susceptible to 3*d* transition-metal substitution and magnetic field.

I. INTRODUCTION

Phase competition is essential to the emergent magnetic and electronic properties of transition-metal oxide materials. For instance, in the perovskite manganite system $(La_{1-x}Sr_x)_{n+1}Mn_nO_{3n+1}$, the competition between antiferromagnetic superexchange and ferromagnetic double exchange interactions can give rise to the colossal magnetoresistance (CMR) effect with orders of magnitude change in resistivity upon applying a magnetic field [1,2]. The competing phases are generally believed to originate from the strong coupling among electronic spin, charge, orbital, and the lattice degrees of freedom. The delicate balance can be readily tipped by chemical doping, as well as external tuning parameters, such as the magnetic field and pressure, etc., resulting in dramatic changes in the materials' physical properties.

Ruddlesden-Popper series perovskite ruthenate $(Sr_{1-x}Ca_x)_{n+1}Ru_nO_{3n+1}$ is one of the prototypical 4*d* transition-metal oxide systems, where a variety of fascinating phenomena have been observed depending on the dimensionality n and the chemical composition x. The single-layer Sr_2RuO_4 (n = 1) shows unconventional superconductivity with spin-triplet pairing [3,4,5] , and the bilayer $Sr_3Ru_2O_7$ (n = 2) possesses a magnetic-field-tuned metamagnetic quantum critical point [6] and exhibits highly anisotropic magnetotransport properties [7]. Substituting isovalent Ca for Sr results in structural distortions due to its smaller ionic radius, which gives rise to a G-type antiferromagnetic (G-AFM) Mott insulating state in Ca_2RuO_4 [8]. The bilayer ruthenate $Ca_3Ru_2O_7$ has an orthorhombic crystal structure with space group No. 36 $Bb2_1m$ [9]. It undergoes an antiferromagnetic transition at T_N = 56 K and a metal-insulator transition (MIT) at T_{MIT} = 48 K [10]. Below T_N, the magnetic moments are ferromagnetically aligned within the bilayer but antiferromagnetically stacked along the *c* axis. Upon cooling, the staggered magnetic moments switch from the *a* axis (denoted as AFM-a) to the *b* axis (denoted as AFM-b as shown in Fig. 1

(a)) at T_{MIT} [11], which is accompanied by a discontinuous change in the lattice constants of ~ 0.1% [9]. The electronic ground state of this system is a quasi-two-dimensional metal [12], due to small un-nested Fermi surface pockets surviving below 30 K [13]. Similar to $(Ca_{1-x}Sr_x)_2RuO_4$ [14], substitution of Sr for Ca sites in $Ca_3Ru_2O_7$ also gives rise to complex magnetic phase diagrams due to the structural change [15, 16].

Alternatively, we have recently found that substituting 3*d* transition-metal elements for Ru can drastically alter the magnetic and electronic properties of this system and lead to new phases. For instance, upon nonmagnetic Ti substitution, the $Ca_3(Ru_{1-x}Ti_x)_2O_7$ system evolves towards a G-type antiferromagnetic Mott insulating state ($x \geq 0.03$, as shown in Fig. 1(a)), with a significant change in the lattice constants of ~1% at T_{MIT} [17,18]. The Mott nature of the insulating state has been confirmed by hard *x*-ray photoemission measurements [19]. On the other hand, magnetic Fe substitution gives rise to a localized electronic ground state with the magnetic structure showing a coexistence of the commensurate (CM) AFM-b and an incommensurate (ICM) spin structure with nearly temperature-independent magnetic wave vector $\mathbf{q}_{ICM} \sim (0.017\ 0\ 1)$ [20].

Furthermore, the physical properties of both pristine and doped $Ca_3Ru_2O_7$ can be readily tuned by the magnetic field. For $Ca_3Ru_2O_7$, a bulk spin valve effect is observed when the magnetic field is applied along the *b* axis, where a change of ~1 order of magnitude in the magnetoresistance occurs at B = 6 T, together with a metamagnetic transition to a canted antiferromagnetic state (CAFM, as shown in Fig. 1(a)) [11,21]. In addition, when the field is along the *a* axis, the resistivity changes by ~3 orders of magnitude at B = 15 T, accompanied by a structural transition, which is ascribed to the change in the orbital occupancy of Ru t_{2g} levels [21]. Very intriguingly, for Ti-doped $Ca_3Ru_2O_7$ the Mott insulating ground state unusually collapses in

a magnetic field, which occurs simultaneously with a magnetic transition to CAFM and a structural change. The resulting colossal change in the magnetoresistance has been suggested to be fundamentally different from the CMR reported in the phase-separated manganites [22].

The sensitivity of the ground state properties of $Ca_3Ru_2O_7$ with respect to modest chemical doping and magnetic field unambiguously suggests that there exist competing phases in this bilayer ruthenate system. And both the temperature- and field-induced phase transitions observed in pure and Ti-doped compounds indicate a strong interplay among spin, lattice, and charge degrees of freedom in this system. Furthermore, the significant difference in the effects of nonmagnetic Ti and magnetic Fe doping on the ground state properties raises an interesting question: what is the role of the 3*d* dopants in determining the magnetic and electronic states?

In this paper, we report the doping effects of another magnetic impurity Mn on the magnetic structure of $Ca_3Ru_2O_7$. We find that Mn induces an ICM cycloidal magnetic structure in the narrow temperature range close to T_{MIT} for $x \leq 0.03$, while the ground state magnetic structure is the same as that of the parent compound. However, the system exhibits a G-type antiferromagnetic Mott insulating state, with a simultaneous change in the lattice parameters at T_{MIT} for $x \geq 0.04$. Furthermore, in $Ca_3(Ru_{0.96}Mn_{0.04})_2O_7$ that is close to the phase boundary [23], a magnetic field applied along the *b* axis drives a spin structure transition from G-AFM to CAFM below T_{MIT}, which is accompanied by an insulator-to-metal transition (IMT) and a drastic change in lattice parameters. In contrast, for $T_{MIT} < T < T_{ICM}$, an ICM-to-CM magnetic transition has been observed without any observable structural change. Our results show that the effect of the magnetic Mn doping is very similar to that of nonmagnetic Ti doping, but different from the magnetic Fe doping. This study demonstrates the importance of phase competition in determining the physical properties of this bilayer ruthenate system, as well as the effectiveness

of 3*d* transition-metal doping and magnetic field in tuning the delicate balance among the competing states.

II. EXPERIMENT

The single-crystal samples of $Ca_3(Ru_{1-x}Mn_x)_2O_7$ with doping concentrations ranging from $x = 0$ to $x = 0.1$ were grown by the floating zone technique. The magnetization and resistivity measurements were performed using the Physical Property Measurement System (PPMS, Quantum Design). Neutron diffraction experiments were carried out using the HB-1A and CG-4C triple-axis spectrometers at High Flux Isotope Reactor (HFIR) in Oak Ridge National Laboratory. The energy of the incident neutrons of HB-1A and CG-4C was fixed as $E_i = 14.6$ meV and 5 meV, respectively. During the measurements on samples of different doping concentrations at zero field, the samples were oriented in (H 0 L) and (0 K L) scattering planes, where H, K and L are in reduced lattice units (r.l.u.) $2\pi/a$, $2\pi/b$ and $2\pi/c$. Samples were mounted in an aluminum sample can and cooled down using a closed-cycle Helium refrigerator down to 4 K. To study the magnetic-field-induced transition, the $Ca_3(Ru_{0.96}Mn_{0.04})_2O_7$ sample was aligned in the horizontal (H 0 L) scattering plane and loaded into a vertical-field cyromagnet such that the magnetic field was applied along the b axis up to 8 T.

III. RESULTS AND DISCUSSION

A. Magnetic properties of $Ca_3Ru_2O_7$ upon Mn doping at zero field.

Figure 2 shows the temperature dependence of the intensity of the representative magnetic Bragg peaks for Mn-doped $Ca_3Ru_2O_7$ with different doping concentration x. For $x = 0.03$, at $T_N \sim 61$ K the magnetic Bragg peaks show up continuously at the nuclear-forbidden wave vectors **q** = (0 0 1) and its equivalent positions, for example (0 0 5), (0 0 7) etc., in the reciprocal space. The intensity keeps increasing until $T_{ICM} \sim 42$ K, where an ICM magnetic

Bragg peak $\mathbf{q}_{ICM}$ = (δ 0 1) emerges while the CM ones get suppressed. This ICM magnetic structure only exists in a very narrow temperature range T_{CM} (~ 34 K) < T < T_{ICM}, below which the intensity of the CM magnetic peaks is enhanced and persists down to the lowest temperature measured. For x = 0.04, the high-temperature magnetic transitions are similar to that of x = 0.03, however, at T_{MIT} ~ 30 K the intensity of both (0 0 1) and (δ 0 1) completely disappears and new magnetic peaks show up at (1 0 2), (1 0 4) and (1 0 6) etc., which suggests that the ground state magnetic structure is different from that of the parent compound and the x = 0.03 one. For x = 0.05, only one first-order magnetic transition is seen at T_N ~ 60 K, and the low-temperature magnetic structure is characterized by the magnetic peak **q** = (1 0 2).

To determine the spin structures of the different magnetic phases in Mn-doped $Ca_3Ru_2O_7$ compounds, we have collected a series of nuclear and magnetic Bragg peaks in (H 0 L) and (0 K L) scattering planes for each Mn doping concentration. Figure 3(a)-3(d) show the neutron diffraction scans along the [1 0 0] direction across the magnetic Bragg peak (0 0 5) and (0 0 1) for x = 0.03 and 0.04 at representative temperatures, and the rocking curve scans over (1 0 2) for x = 0.04 and 0.05 are shown in Fig. 3(e) and 3(f) respectively. We have performed magnetic representation analysis to explore the possible magnetic structures using the Rietveld refinement package FULLPROF [[24]]. We find that the strongest (0 0 1) peak corresponds to an antiferromagnetic structure where the magnetic moments are aligned parallel to each other within the bilayer, but antiparallel between adjacent bilayers (AFM-a or AFM-b) [[11]]. And the strongest (1 0 2) peak represents a G-type antiferromagnetic structure with all nearest-neighbor magnetic moments aligned antiparallel to each other (G-AFM) [[17]]. The ICM magnetic phase characterized by the magnetic wave vector (δ 0 1) is a cycloidal magnetic structure propagating along the a axis, with the period determined by the incommensurability δ. It is worth noting that the

magnetic wave vectors of the ICM magnetic structures are strongly temperature dependent, as shown in Figure 3(c) and 3(d). No higher-order harmonics are observed, suggesting that the ICM magnetic structure is uniformly modulated (Fig. 1(c)), in contrast to the magnetic soliton lattice in the Fe-doped compound [20]. For x = 0.03, similar to the parent compound, the (2 0 1) magnetic peak is present at T = 4 K but is absent at 50 K, which suggests that at $T < T_{CM}$ the magnetic moments are along the b axis (AFM-b), while in the high-temperature phase $T_{ICM} < T < T_N$ the moments are along the a axis (AFM-a) [11] which is also the case for x = 0.04.

Very intriguingly, the magnetic transition to the low-temperature G-AFM state is accompanied by a dramatic change in the lattice constants. Figure 4 shows the lattice constants a, b and c as a function of temperature. For x = 0.03, there is no observable anomaly in all the lattice constants throughout the temperature range measured. In contrast, for x = 0.04, upon cooling the lattice constants b increases discontinuously by ~0.98% while c decreases by ~0.71% at T_{MIT} ~ 30 K, which is much more pronounced compared with that in the parent compound (~0.1%) [9]. The shortening along the c axis and the expansion in the in-plane b axis results in a flattening of the RuO_6 octahedron, similar to that in the single-layer Ca_2RuO_4, which may indicate a change in the orbital occupancy of the Ru t_{2g} electrons [25,26]. For x = 0.05, a structural change of comparable magnitude is also observed at the magnetic transition at T_N.

B. Magnetic and transport properties of $Ca_3(Ru_{1-x}Mn_x)_2O_7$ (x = 0.04) in the presence of magnetic field.

We have further investigated the effect of the magnetic field on the magnetic and electronic properties of Mn-doped $Ca_3Ru_2O_7$. Note that since the ground state magnetic structure of x = 0.03 compound is similar to the parent compound (AFM-b), applying a magnetic field along the b axis is expected to lead to a transition to CAFM [11]. In contrast, no field-induced

transition (up to 9 T) is observed in the resistivity measurements on the $x = 0.05$ sample (data not shown). Notably, the $x = 0.04$ compound is close to the phase boundary [23], bridging the correlated AFM-b phase and the Mott insulating G-AFM state. Therefore, we have performed single-crystal neutron diffraction, magnetization and resistivity measurements on Mn-doped $Ca_3Ru_2O_7$ of this doping concentration ($x = 0.04$).

Figure 5(a) shows the temperature dependence of the in-plane resistivity ρ_{ab} of Mn-doped $Ca_3Ru_2O_7$ ($x = 0.04$) in 0 T and 9 T applied along the b axis, respectively. In contrast to the zero-field data where a series transitions have been observed, in a magnetic field of 9 T, the system displays a localized behavior throughout the entire temperature range measured, suggesting a dramatic change in the electronic structure. In addition, the field-induced IMT is accompanied by magnetic transitions. Figure 5(b) and 5(c) show the isothermal magnetoresistance and magnetization as a function of magnetic field at $T = 10$ K and 34 K, respectively. At $T = 10$ K, the Mott insulating ground state is suppressed by a magnetic field at $B_c^{\uparrow} \sim 7.2$ T with a change in the resistivity by ~ 3 orders of magnitude. Concurrently, a large change in magnetization is observed, indicating a field-induced spin structure transition. The field-induced phase transition is of first-order, which is manifested by the large hysteretic effect as the magnetic field increases and decreases. At $T = 34$ K, where the zero-field state shows the coexistence of CM and ICM magnetic structures, the magnetic field can also drive a first-order-like magnetic transition, as shown in both the magnetoresistance and magnetization measurements. However, a much smaller change in resistivity is observed upon applying the field, presumably related to the spin scattering effect associated with the change in the magnetic structure, which is distinct from the $T = 10$ K data that arises from the change in electronic structure.

In order to determine the spin structure of the field-induced state in Mn-doped $Ca_3Ru_2O_7$ (x = 0.04), we performed neutron diffraction measurements. Figure 6(a) and 6(b) show the rocking curve scans across magnetic wave vectors **q** = (1 0 2) and (0 0 1) at T = 10 K, B = 0 T and 8 T, respectively. One clearly sees that (1 0 2) peak is suppressed completely at 8 T, while an alternative magnetic Bragg peak (0 0 1) shows up. Figure 6(c) and 6(d) show the intensity of **q** = (1 0 2) and (0 0 1) magnetic Bragg peaks as a function of magnetic field at T = 10 K. A field-induced magnetic structure transition is observed at $B_c^{\uparrow}$ = 7.3 ± 0.1 T. The large hysteresis observed when the magnetic field increases and decreases indicates the first-order nature of the field-induced spin structure transition, in agreement with both magnetoresistance and magnetization measurements (Fig. 5(b)). We have collected a series of magnetic Bragg peaks such as (0 0 3), (0 0 5), (2 0 1) *et al*. at B = 8 T, and performed representation analysis using FULLPROF [24]. The antiferromagnetic structure that best describes the neutron diffraction data is of AFM-a type, where the staggered magnetic moments are along the *a* axis, perpendicular to the applied magnetic field. In combination to the ferromagnetic component along the *b* axis revealed in the magnetization measurements (Fig. 5(b)), the resultant field-induced magnetic state is a canted antiferromagnetic structure (CAFM, Fig. 1(a)), a vector sum of the AFM-a type antiferromagnetic component and a ferromagnetic component (~1.4 μ_B at B = 8 T, 10 K) along the *b* axis, similar to the field-induced state in the parent and Ti-doped compound [11,22]. It is worth noting that above $B_c^{\uparrow}$, the intensity of (0 0 1) starts to decrease as the magnetic field increases further, which can be ascribed to the fact that CAFM transforms towards the fully polarized state (PM) with a decrease in the staggered antiferromagnetic moment.

We have also studied the field-induced magnetic transition of the ICM magnetic structures at $T_{MIT} < T < T_{ICM}$. Figure 7(a) and 7(b) show scans along the [1 0 0] direction across

the magnetic Bragg peak **q** = (0 0 1) at T = 34 K. At zero field, the magnetic structure exhibits the consistence of CM and ICM phases. However, at B = 5 T, the ICM peaks are suppressed, and the intensity of the CM peak becomes much stronger, indicating an ICM-to-CM transition. Similar enhancements in the magnetic intensity are also observed at the wave vectors (0 0 3), (0 0 5) and (0 0 7) *et al* (data now shown). Figure 7(c) and 7(d) shows the field dependence of magnetic intensity of **q** = (0 0 1) and (0.0245 0 1) at T = 34 K. The system undergoes an ICM-to-CM magnetic transition at $B_{c1}^{\uparrow}$ = 4.4 ± 0.1 T, where the (0.0245 0 1) peak is suppressed completely and the (0 0 1) peak increases then stays almost constant. This field-induced ICM-CM transition is also of first-order in nature, as the hysteresis loops are clearly seen when the magnetic field increases and decreases. By performing an analysis similar to that at T = 10 K, we conclude that the field-induced magnetic state at $B_{c1}^{\uparrow}$ is CAFM (Fig. 1(a)) as well. In addition, as the magnetic field increases further, the intensity of the (0 0 1) peak starts to decrease and finally disappears at $B_{c2}^{\uparrow}$ = 6.6 T, which indicates that the AFM-a component of the CAFM state is completely suppressed and the system is in a fully spin polarized state (PM).

The field-induced IMT of the G-AFM Mott insulating state is accompanied by a simultaneous change in the lattice parameters. As shown in Figure 8(a), at T = 10 K, the lattice parameter c increases at $B_c^{\uparrow}$ by nearly ~1%, while the lattice constant a remains unchanged across the transition. The magnetoelastic coupling is similar to that observed at zero field, where the Mott insulating state is accompanied by a flattening of the RuO_6 octahedra. On the contrary, no crystal structural change is observed for the field-induced magnetic transition at T = 34 K, as shown in Figure 8(b).

C. Discussions

We have investigated the magnetic properties of Mn-doped $Ca_3Ru_2O_7$ as a function of temperature T and Mn doping concentration x. Very surprisingly, the effect of magnetic Mn doping resembles that of the nonmagnetic Ti substitution [18], but is contrasted with the magnetic Fe doping effect [20]. This suggests that these emergent states are related to the intrinsic instabilities of the Ru-O network and the role of the 3*d* dopants is to tip the balance between different competing tendencies which already exist in this bilayer ruthenate system.

There are several interesting features found in Mn-doped $Ca_3Ru_2O_7$ that are worth further discussion. Firstly, the emergence of the ICM magnetic structure upon light Mn doping. It seems that the ICM magnetic structure is a common feature in 3*d* transition-metal doped $Ca_3Ru_2O_7$ [18,20], suggesting the strong competition between the AFM-b and ICM magnetic phases in this bilayer ruthenate. The ICM magnetic structure is most probably ascribable to the Dzyaloshinskii-Moriya interaction (DM), as Mn-doped $Ca_3Ru_2O_7$ has a noncentrosymmetric space group (No. 36 $Bb2_1m$) [9]. The competition among DM interaction, antiferromagnetic superexchange, ferromagnetic double exchange interaction [27] and magnetocrystalline anisotropy, can give rise to either a collinear magnetic structures as in the pristine compound [11], or a modulated magnetic structure with noncollinear spin arrangement as in the doped ones.

Secondly, the emergence of the G-type antiferromagnetic Mott insulating state for $x \geq 0.04$. A similar ground state has been observed in the single-layer Ca_2RuO_4 and Ti-doped $Ca_3Ru_2O_7$ [28,17], but not in the parent or Fe-doped compound [11,20]. A comparison among these compounds leads to several important implications to the stabilization of such a phase. (i) The electron correlation is essential to realize the insulating state, as density functional theory calculations without the on-site Coulomb repulsion fail to capture the insulating nature of the ground state Ti-doped $Ca_3Ru_2O_7$ [17], while an inclusion of onsite Coulomb repulsion U = 2 eV

results in an opening of the electronic gap [22]. Furthermore, the Mott-type scenario is also supported by the hard *x*-ray photoemission measurements [19]. (ii) There is strong coupling between spin and lattice degrees of freedom. The G-AFM structure is always accompanied by a discontinuous change in the lattice constants of the order ~1% at T_{MIT}, which results in a considerable flattening of the RuO_6 octahedra. In contrast, in the materials whose ground state magnetic structure is AFM-b or ICM, the change in the lattice parameters are much smaller (e.g. ~0.1% in the parent compound [9]) or not observable (e.g. Fe-doped $Ca_3Ru_2O_7$ [20] and $Ca_3(Ru_{0.97}Mn_{0.03})_2O_7$). In a recent report, applying hydrostatic pressure is shown to induce a magnetic structure transition from G-AFM to AFM-b in Ti-doped $Ca_3Ru_2O_7$ [29], suggesting a direct correlation between G-AFM and the crystalline lattice in this bilayer ruthenate. Microscopically, the correlation between magnetism and crystal structure have been studied theoretically on Ca_2RuO_4 and it is revealed that the rotation of RuO_6 favors ferromagnetism and the subsequent tilting favors antiferromagnetism [26]. Similar conclusions are expected to hold for the Mn-doped $Ca_3Ru_2O_7$ because of the similar layered structure. (iii) The flattening of the RuO_6 octahedra is expected to change the orbital occupancy of the Ru t_{2g} level. For a multiband Mott-Hubbard system, the orbital polarization is suggested to be closely associated with the Mott transition by suppressing the orbital fluctuations [30,31]. Experimentally, ferro-type orbital order has been observed in Ca_2RuO_4 system by resonant *x*-ray scattering [32]. In a recent study on Ti-doped $Ca_3Ru_2O_7$, density functional theory calculations suggest an orbital polarization in the G-AFM Mott insulating state, where the spin down channel of in-plane d_{xy} orbital is fully occupied and that of out-of-plane d_{xz}/d_{yz} orbitals are almost empty, leading to the gap opening with an electronic configuration d_{xy} ($\downarrow\uparrow$) and d_{xz}/d_{yz}($\uparrow$,$\uparrow$). On the contrary, in the AFM-b phase with a longer *c* axis and shorter *b* axis, the calculations shows no sign of orbital polarization and there is

finite density of states near the Fermi surface [22]. Therefore, the G-AFM Mott insulating states in Ti- and Mn-doped $Ca_3Ru_2O_7$ is a cooperative effect as a result of the coupling among spin, lattice and orbital degrees of freedom.

Thirdly, the similarity in the doping effect of nonmagnetic Ti and magnetic Mn on $Ca_3Ru_2O_7$, which is significantly different from that of the other magnetic dopants Fe. Understanding the effects of 3*d* transition-metal dopants on the emergent phases of the 4*d* layered ruthenates is intriguing but challenging. In a recent work, J. Peng *et al* [23] found that the MIT temperatures T_{MIT} of $Ca_3Ru_2O_7$ with different 3*d* transition-metal dopants are predominated by the structural parameter $c/\sqrt{ab}$, not only in the low-temperature ordered phase, but also in the high-temperature paramagnetic state. It was proposed that the magnetic and electronic states of 3*d* transition-metal doped $Ca_3Ru_2O_7$ is determined by lattice-orbital coupling, i.e., the G-AFM Mott insulating state can only stabilize below a critical value of this structural control parameter, where orbital polarization is expected based on first principles calculations. Therefore, due to the larger structural distortion induced by Ti and Mn dopants compared to that of Fe dopant, Ti- and Mn-doped $Ca_3Ru_2O_7$ compounds exhibit G-AFM Mott insulating state, whereas the Fe-doped compound shows incommensurate magnetic structure resulting from the competition between DM interaction, exchange interactions, and magnetic anisotropy, and electronically it is a localized state induced by Fe impurities. Furthermore, it has been suggested that the structural distortions caused by 3*d* transition-metal impurity is dominated by electronic scattering, rather than the difference in the ionic radius or magnetic moments [23].

Finally, the collapse of the Mott insulating state in a magnetic field. It is quite unusual to observe a magnetic-field-induced IMT in a Mott insulator since early theoretical studies on a single-band Mott-Hubbard Hamiltonian reveal that the magnetic field tends to stabilize the

insulating state by a first-order metamagnetic phase transition [33], which has been observed experimentally in systems such as organic superconductors [34]. The discrepancies in the theoretical predictions and the observations in Mn-doped $Ca_3Ru_2O_7$ may arise from the fact that the Mott transition in ruthenates is more complicated by a number of factors that are absent in the simplest model considered. As discussed previously, the Mott transition in these ruthenates involves three t_{2g} bands, which indicates that orbital degrees of freedom may be important to the Mott transition. In addition, the IMT is accompanied by the simultaneous change in magnetic and crystal structures. There are several key aspects that are likely to be essential to understanding the field-induced IMT in Mn-doped $Ca_3Ru_2O_7$. (i) Phase competition. Mn-doped $Ca_3Ru_2O_7$ (x = 0.04) is close to the phase boundary, which implies the presence of strong magnetic and electronic instabilities. The balance of competition between two highly distinct magnetic and electronic states, e.g. G-AFM Mott insulating state and CAFM weakly localized state, can be easily tuned by the magnetic field. This is supported by the fact that for x = 0.05 compound that is away from the phase boundary, the magnetic field up to 9 T cannot drive an IMT. (ii) The coupling between spin, lattice and orbital degrees of freedom. In a magnetic field applied along the easy axis, the introduction of the Zeeman energy leads to a magnetic structure transition from G-AFM to CAFM, which would cause a simultaneous change in the lattice constants and possibly orbital occupancy as discussed above, and gives rise to drastic effects on the electronic properties of this material.

IV. CONCLUSION

In summary, we have investigated the magnetic properties of the new phases in the bilayer ruthenate $Ca_3Ru_2O_7$ induced by Mn doping. The system shows an ICM magnetic structure for $x \leq 0.03$, where the ground state magnetic structure is the same as the parent

compound. For $x \geq 0.04$, the ground state changes to a G-type antiferromagnetic Mott insulator. We have also investigated the magnetic-field-induced phase transitions in Mn-doped $Ca_3Ru_2O_7$ for $x = 0.04$ that is positioned at the T - x phase boundary. Upon applying magnetic field, the G-AFM ground state transforms into CAFM through a first-order transition, together with a collapse of the Mott insulating state and drastic changes in the lattice constants. Our results unambiguously demonstrate the competition between various states in this bilayer ruthenate system, which can be tuned by 3*d* transition-metal doping and external magnetic field.

Acknowledgments

The work at Michigan State University was supported by the National Science Foundation under Award No. DMR-1608752 and the start-up funds from Michigan State University. The work at Tulane is supported by the U.S. Department of Energy under EPSCoR Grant No. DE-SC0012432 with additional support from the Louisiana Board of Regents and work at ORNL was supported by the Scientific User Facilities Division, Office of Basic Energy Sciences, DOE. Work at Nanjing University was supported by the National Natural Science Foundation of China (No. 11304149).

Figure Captions

Figure 1. (a) Schematics of the crystal and magnetic structures of Mn-doped $Ca_3Ru_2O_7$. AFM-b: ferromagnetic bilayers coupled antiparallel along the *c* axis. The staggered magnetic moments are along the *b* axis. G-AFM: the nearest-neighbor magnetic moments are antiferromagnetic. CAFM: canted antiferromagnetic structure consisting of an antiferromagnetic component (AFM-a) and a ferromagnetic component along the *b* axis. (b),(c) In-plane view of one RuO_2 layer of AFM-b and ICM cycloidal magnetic structures, respectively.

Figure 2. Temperature dependence of the intensity of the representative magnetic Bragg peaks (1 0 2), (0 0 1) and (0.0246 0 1), of $Ca_3(Ru_{1-x}Mn_x)_2O_7$ (x = 0.03, 0.04, and 0.05).

Figure 3. (a),(b) Neutron diffraction scans along the [1 0 0] direction across the magnetic wave vector (0 0 5) at representative temperatures. Note that H is in reduced lattice unit (r.l.u.). (c),(d) Neutron diffraction scans across the magnetic wave vector (0 0 1) in the ICM magnetic phase. (e),(f) Rocking curve scans across the magnetic wave vector (1 0 2) at representative temperatures.

Figure 4. Lattice parameters as a function of temperature $Ca_3(Ru_{1-x}Mn_x)_2O_7$ (x = 0.03 and 0.04).

Figure 5. (a) Temperature dependence of the in-plane resistivity ρ_{ab} at B = 0 T and 9 T, B // b axis. (b),(c) Field dependence of the in-plane resistivity ρ_{ab} and magnetization M_b at T = 10 K and 34 K, B // b axis.

Figure 6. (a),(b) Rocking curve scans on $Ca_3(Ru_{1-x}Mn_x)_2O_7$ (x = 0.04) across **q** = (1 0 2) and (0 0 1) at B = 0 T and 8 T, respectively, T = 10 K. (c),(d) The intensity of **q** = (1 0 2) and (0 0 1) magnetic Bragg peak as a function of magnetic field, T = 10 K.

Figure 7. (a),(b) Neutron diffraction scan on $Ca_3(Ru_{1-x}Mn_x)_2O_7$ (x = 0.04) along [1 0 0] direction across the magnetic Bragg peak **q** = (0 0 1) at B = 0 T and 5 T, T = 34 K. Note that H is in reduced lattice unit (r.l.u.). (c),(d) The intensity of **q** = (0 0 1) and (0.0245 0 1) magnetic Bragg peaks as a function of magnetic field, T = 34 K.

Figure 8. Lattice constants a and c as a function of magnetic field at (a) T = 10 K (b) T = 32 K.

Figure 1

M. Zhu *et al*,

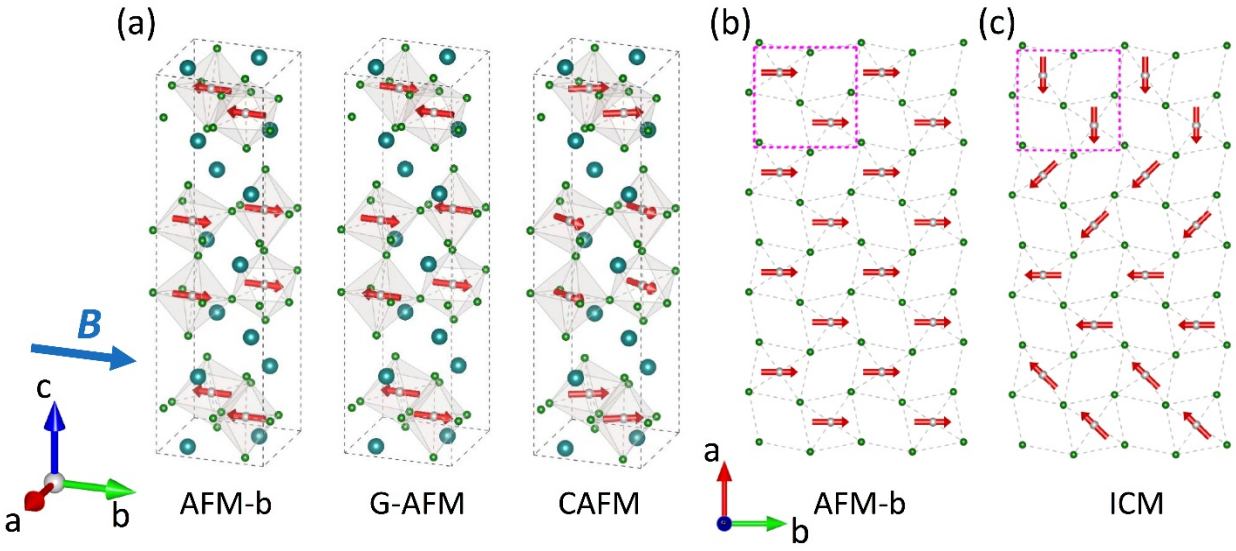

Figure 2

M. Zhu *et al*,

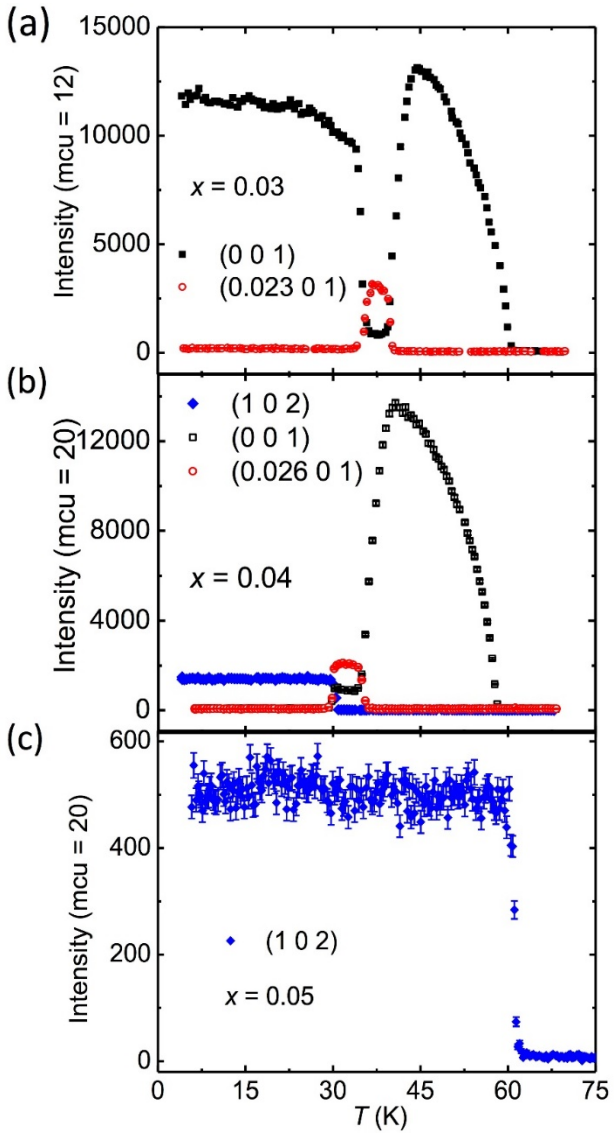

Figure 3

M. Zhu *et al*,

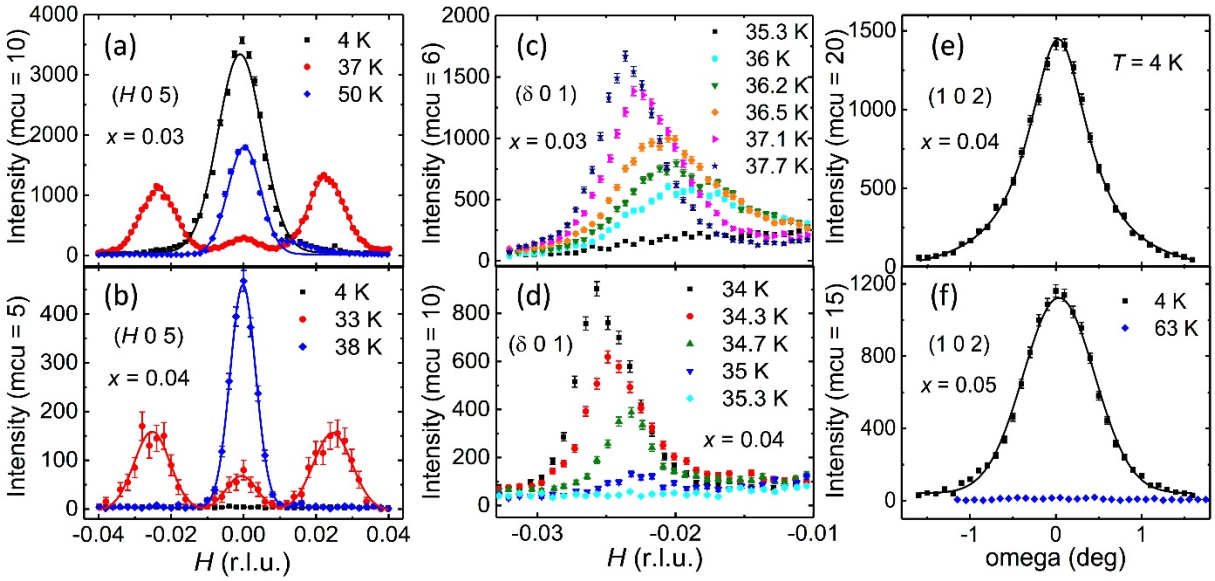

Figure 4

M. Zhu *et al*,

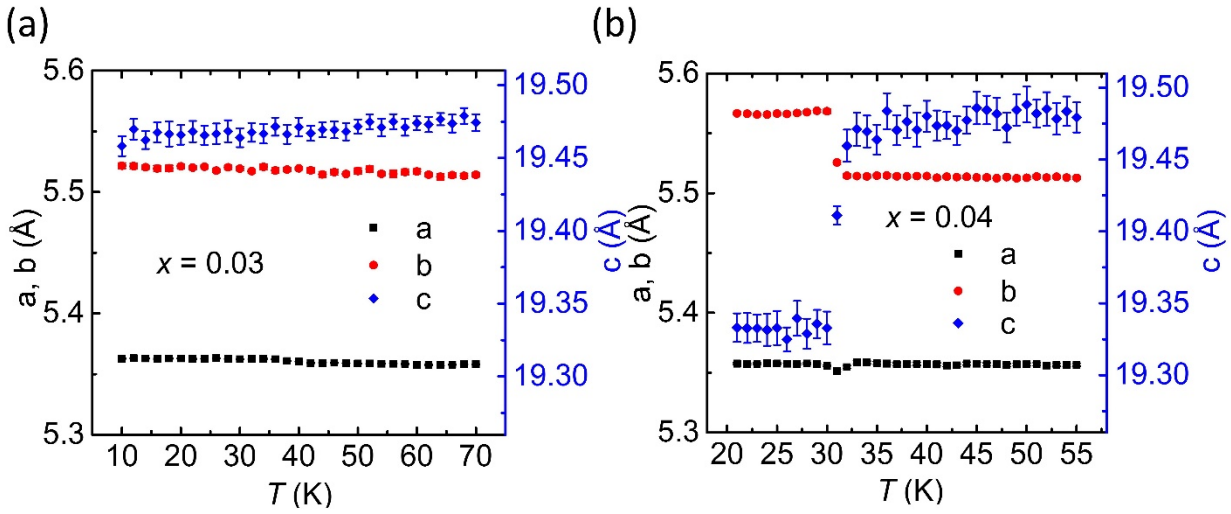

Figure 5

M. Zhu *et al*,

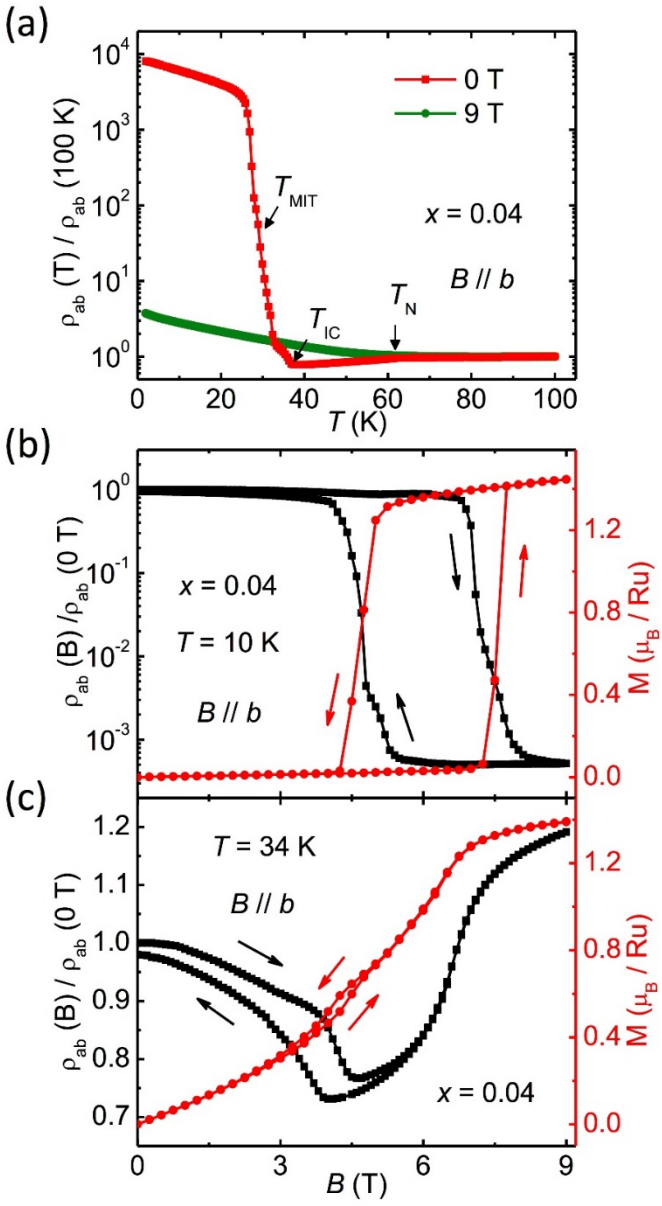

Figure 6

M. Zhu *et al*,

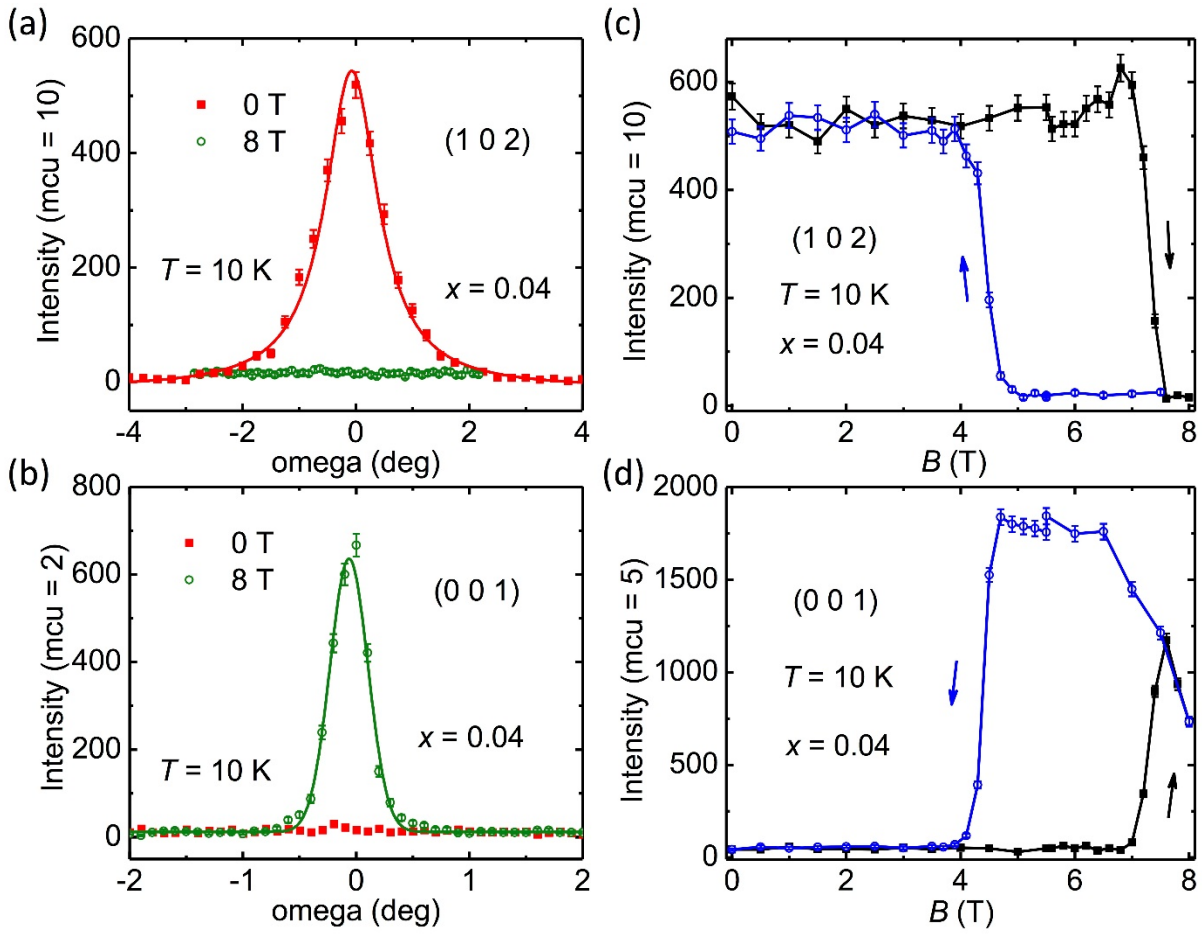

Figure 7

M. Zhu et al.

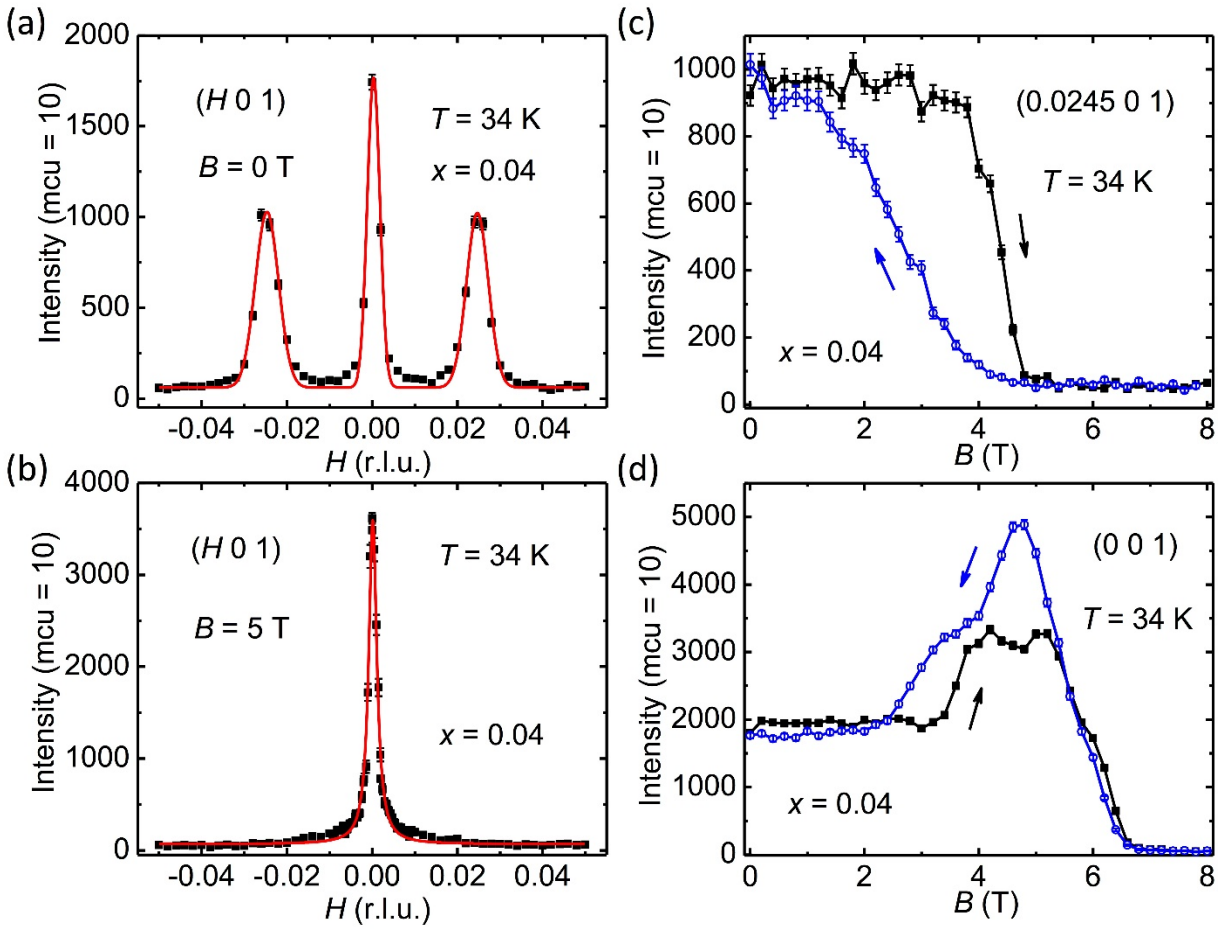

Figure 8

M. Zhu et al.

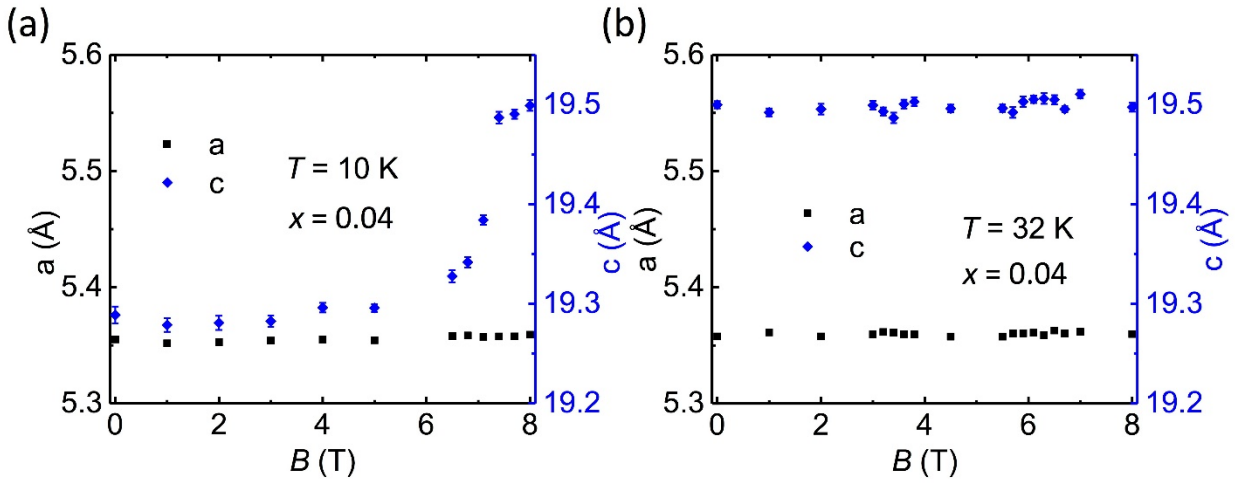

[1] Y. Tokura, Y. Tomioka, H. Kuwahara, A. Asamitsu, Y. Moritomo, and M. Kasai, Journal of Applied Physics **79** (8), 5288 (1996).
[2] Myron B. Salamon and Marcelo Jaime, Reviews of Modern Physics **73** (3), 583 (2001).
[3] Andrew Peter Mackenzie and Yoshiteru Maeno, Reviews of Modern Physics **75** (2), 657 (2003).
[4] Yoshiteru Maeno, Shunichiro Kittaka, Takuji Nomura, Shingo Yonezawa, and Kenji Ishida, Journal of the Physical Society of Japan **81** (1), 011009 (2011).
[5] Ying Liu and Zhi-Qiang Mao, Physica C: Superconductivity and its Applications **514**, 339 (2015).
[6] S. A. Grigera, R. S. Perry, A. J. Schofield, M. Chiao, S. R. Julian, G. G. Lonzarich, S. I. Ikeda, Y. Maeno, A. J. Millis, and A. P. Mackenzie, Science **294** (5541), 329 (2001).
[7] R. A. Borzi, S. A. Grigera, J. Farrell, R. S. Perry, S. J. Lister, S. L. Lee, D. A. Tennant, Y. Maeno, and A. P. Mackenzie, Science **315** (5809), 214 (2007).
[8] Satoru Nakatsuji, Shin-ichi Ikeda, and Yoshiteru Maeno, Journal of the Physical Society of Japan **66** (7), 1868 (1997).
[9] Yoshiyuki Yoshida, Shin-Ichi Ikeda, Hirofumi Matsuhata, Naoki Shirakawa, C. H. Lee, and Susumu Katano, Physical Review B **72** (5), 054412 (2005).
[10] G. Cao, S. McCall, J. E. Crow, and R. P. Guertin, Physical Review Letters **78** (9), 1751 (1997).
[11] Wei Bao, Z. Q. Mao, Z. Qu, and J. W. Lynn, Physical Review Letters **100** (24), 247203 (2008).
[12] Yoshiyuki Yoshida, Ichiro Nagai, Shin-Ichi Ikeda, Naoki Shirakawa, Masashi Kosaka, and Nobuo Môri, Physical Review B **69** (22), 220411 (2004).
[13] F. Baumberger, N. Ingle, N. Kikugawa, M. Hossain, W. Meevasana, R. Perry, K. Shen, D. Lu, A. Damascelli, A. Rost, A. Mackenzie, Z. Hussain, and Z. X. Shen, Physical Review Letters **96** (10), 107601 (2006).
[14] S. Nakatsuji and Y. Maeno, Physical Review Letters **84** (12), 2666 (2000).
[15] Zhe Qu, Jin Peng, Tijiang Liu, David Fobes, Leonard Spinu, and Zhiqiang Mao, Physical Review B **80** (11), 115130 (2009).
[16] Zhe Qu, Jin Peng, Tijiang Liu, David Fobes, Vlad Dobrosavljević, Leonard Spinu, and Z. Q. Mao, Physical Review B **86** (1), 014434 (2012).
[17] X. Ke, J. Peng, D. J. Singh, Tao Hong, Wei Tian, C. R. Dela Cruz, and Z. Q. Mao, Physical Review B **84** (20), 201102 (2011).
[18] Jin Peng, X. Ke, Gaochao Wang, J. E. Ortmann, David Fobes, Tao Hong, Wei Tian, Xiaoshan Wu, and Z. Q. Mao, Physical Review B **87** (8), 085125 (2013).
[19] S. Tsuda, N. Kikugawa, K. Sugii, S. Uji, S. Ueda, M. Nishio, and Y. Maeno, Physical Review B **87** (24), 241107(R) (2013).
[20] X. Ke, J. Peng, W. Tian, Tao Hong, M. Zhu, and Z. Q. Mao, Physical Review B **89** (22), 220407 (2014).
[21] E. Ohmichi, Y. Yoshida, S. I. Ikeda, N. Shirakawa, and T. Osada, Physical Review B **70** (10), 104414 (2004).
[22] M. Zhu, J. Peng, T. Zou, K. Prokes, S. D. Mahanti, T. Hong, Z. Q. Mao, G. Q. Liu, and X. Ke, Physical Review Letters **116** (21), 216401 (2016).
[23] J. Peng et al. unpublished (2016).
[24] Juan Rodríguez-Carvajal, Physica B: Condensed Matter **192** (1–2), 55 (1993).

[25] O. Friedt, M. Braden, G. André, P. Adelmann, S. Nakatsuji, and Y. Maeno, Physical Review B **63** (17), 174432 (2001).
[26] Z. Fang and K. Terakura, Physical Review B **64** (2), 020509 (2001).
[27] D. Singh and S. Auluck, Physical Review Letters **96** (9), 097203 (2006).
[28] M. Braden, G. André, S. Nakatsuji, and Y. Maeno, Physical Review B **58** (2), 847 (1998).
[29] T. Zou, H. B. Cao, G. Q. Liu, J. Peng, M. Gottschalk, M. Zhu, Y. Zhao, J. B. Leão, W. Tian, Z. Q. Mao, and X. Ke, Physical Review B **94** (4), 041115 (2016).
[30] A. Liebsch and H. Ishida, Physical Review Letters **98** (21), 216403 (2007).
[31] E. Gorelov, M. Karolak, T. O. Wehling, F. Lechermann, A. I. Lichtenstein, and E. Pavarini, Physical Review Letters **104** (22), 226401 (2010).
[32] M. Kubota, Y. Murakami, M. Mizumaki, H. Ohsumi, N. Ikeda, S. Nakatsuji, H. Fukazawa, and Y. Maeno, Physical Review Letters **95** (2), 026401 (2005).
[33] Laurent Laloux, Antoine Georges, and Werner Krauth, Physical Review B **50** (5), 3092 (1994).
[34] F. Kagawa, T. Itou, K. Miyagawa, and K. Kanoda, Physical Review Letters **93** (12), 127001 (2004).